



Article

Analysis of Local and Global Aromaticity in Si₃C₅ and Si₄C₈ Clusters. Aromatic Species Containing Planar Tetracoordinate Carbon

Juan J. Torres-Vega ¹, Diego R. Alcoba ^{2,3}, Ofelia B. Oña ⁴, Alejandro Vásquez-Espinal ⁵, Rodrigo Báez-Grez ⁵, Luis Lain ⁶, Alicia Torre ⁶, Víctor García ^{7,*}  and William Tiznado ^{5,*} 

- ¹ Centro de Investigaciones Tecnológicas, Biomédicas y Medioambientales, Calle José Santos Chocano 199, Urb. San Joaquín, Callao 07006, Peru; ikkysams@gmail.com
- ² Departamento de Física, Facultad de Ciencias Exactas y Naturales, Universidad de Buenos Aires, Ciudad Universitaria, Buenos Aires 1428, Argentina; dalcoba@df.uba.ar
- ³ Instituto de Física de Buenos Aires, Consejo Nacional de Investigaciones Científicas y Técnicas, Ciudad Universitaria, Buenos Aires 1428, Argentina
- ⁴ Instituto de Investigaciones Fisicoquímicas Teóricas y Aplicadas, Universidad Nacional de La Plata, CCT La Plata, Consejo Nacional de Investigaciones Científicas y Técnicas, Diag. 113 y 64 (S/N), Sucursal 4, CC 16, La Plata 1900, Argentina; ofelia@inifta.unlp.edu.ar
- ⁵ Computational and Theoretical Chemistry Group, Departamento de Ciencias Químicas, Facultad de Ciencias Exactas, Universidad Andres Bello, República 498, Santiago 8370251, Chile; alejo64724@gmail.com (A.V.-E.); rodrigo.baez.grez@gmail.com (R.B.-G.)
- ⁶ Departamento de Química Física, Facultad de Ciencia y Tecnología, Universidad del País Vasco, Apdo. 644, E-48080 Bilbao, Spain; luis.lain@ehu.es (L.L.); alicia.torre@ehu.es (A.T.)
- ⁷ Departamento Académico de Fisicoquímica, Facultad de Química e Ingeniería Química, Universidad Nacional Mayor de San Marcos, Lima 15004, Peru
- * Correspondence: victor.garcia@unmsm.edu.pe (V.G.); wtiznado@unab.cl (W.T.)



Citation: Torres-Vega, J.J.; Alcoba, D.R.; Oña, O.B.; Vásquez-Espinal, A.; Báez-Grez, R.; Lain, L.; Torre, A.; García, V.; Tiznado, W. Analysis of Local and Global Aromaticity in Si₃C₅ and Si₄C₈ Clusters. Aromatic Species Containing Planar Tetracoordinate Carbon. *Chemistry* **2021**, *3*, 1101–1112. <https://doi.org/10.3390/chemistry3040080>

Academic Editors: Andrea Peluso and Guglielmo Monaco

Received: 20 August 2021

Accepted: 17 September 2021

Published: 25 September 2021

Publisher's Note: MDPI stays neutral with regard to jurisdictional claims in published maps and institutional affiliations.



Copyright: © 2021 by the authors. Licensee MDPI, Basel, Switzerland. This article is an open access article distributed under the terms and conditions of the Creative Commons Attribution (CC BY) license (<https://creativecommons.org/licenses/by/4.0/>).

Abstract: The minimum energy structures of the Si₃C₅ and Si₄C₈ clusters are planar and contain planar tetracoordinate carbons (ptCs). These species have been classified, qualitatively, as global (π) and local (σ) aromatics according to the adaptive natural density partitioning (AdNDP) method, which is an orbital localization method. This work evaluates these species' aromaticity, focusing on confirming and quantifying their global and local aromatic character. For this purpose, we use an orbital localization method based on the partitioning of the molecular space according to the topology of the electronic localization function (LOC-ELF). In addition, the magnetically induced current density is analyzed. The LOC-ELF-based analysis coincides with the AdNDP study (double aromaticity, global, and local). Moreover, the current density analysis detects global and local ring currents. The strength of the global and local current circuit is significant, involving $4n + 2 \pi$ - and σ -electrons, respectively. The latter implicates the Si-ptC-Si fragment, which would be related to the $3c-2e \sigma$ -bond detected by the orbital localization methods in this fragment.

Keywords: clusters; planar tetracoordinate carbon (ptC); local and global aromaticity; chemical bonding; orbital localization; electron localization function (ELF); electron delocalization; current density analysis

1. Introduction

The concept of aromaticity has been extended over time to coin new features that define a system as aromatic and address a diversity of organic and inorganic systems [1–5]. In this regard, nowadays the concept of aromaticity, π and σ , is used extensively to rationalize the stability of some atomic clusters [6]. Accordingly, the aromaticity well justifies the clusters' highly symmetric and stable structures. So, numerous planar boron clusters [7–9], metal clusters [1,5–7,10–14], and metallabenzenes [15–19] fit well into the concept of aromaticity. Along with π - and σ -aromaticity, multiple local π -aromaticity shows to be a

helpful concept for rationalizing complex conjugate systems, such as polycyclic hydrocarbons or graphene [20,21]. Moreover, it was indicated that the concept of multiple local σ -aromaticity is also applicable in the chemistry of nonagermanide clusters [22].

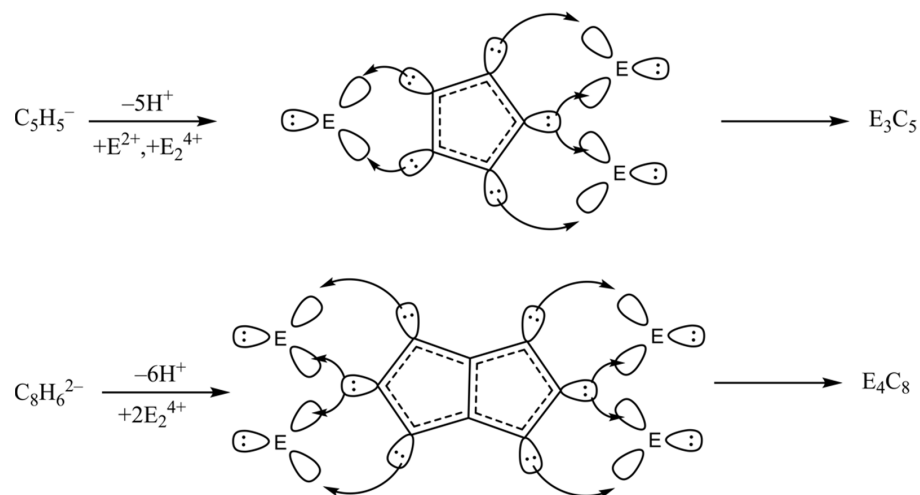
Chemists dedicate considerable effort to predicting new molecules with exotic non-classical structures. Planar hypercoordinate carbons, i.e., carbon linked to four or more ligands in the plane, are especially puzzling systems. With the modest goal of achieving a thermally accessible transition state for a classical racemization experiment, in 1970 Hoffman and coworkers introduced strategies to stabilize a planar tetracoordinate carbon (ptC) [23]. Notably, this study inspired many theoretical and experimental studies over the last 50 years culminating in numerous compounds with ptCs [24–30]. More recently, “planar hypercoordinate” chemistry expanded to include planar species where the central atom is not limited to carbon, and the coordination number is more than four. Species with planar pentacoordinate [31–38] and hexacoordinate [39–42] carbons (ppCs or phCs) have been designed *in silico*. Electronic delocalization (i.e., aromaticity, resonance) plays a determining role in the stability of many of these species. Consequently, a comprehensible chemical bonding analysis is fundamental for interpreting their stability. For instance, the 18-valence electron D_{4h} - CAI_4^{2-} cluster is a doubly σ - and π -aromatic cluster experimentally detected in the $Na^+[CAI_4^{2-}]$ complex [29,30]. Of particular interest in this work is the concept of aromaticity (π , σ , local, global) and the role it plays in justifying the stability of systems with planar hypercoordinate carbons.

Aromaticity is not an observable property, yet it is generally assessed in terms of structural, energetic, and magnetic criteria [3,43–48]. Aromatic and antiaromatic species sustain diatropic and paratropic ring currents when exposed to a uniform magnetic field perpendicular to the molecular plane [49–54]. This magnetic response allows the interpretation of experimental NMR spectroscopy and magnetic anisotropy measurements on (anti) aromatic molecules [45,55]. The nucleus-independent chemical shift (NICS) is a very popular theoretical descriptor used for assessing aromaticity. Schleyer and coworkers defined the NICS as “the negative of the absolute magnetic shielding,” further suggesting to compute it at the molecular center [56]. Note that the Biot–Savart law connects the induced magnetic field at the ring center, and thus the chemical shift at this point, to the ring current density [57]. In particular, the out-of-plane component of the NICS measured above the molecular plane [i.e., $NICS_{zz}(1)$] is well correlated with the intensity of the ring current flux (according to the ring current strength, RCS, values) [58,59]. However, some works reported significant discrepancies between the NICS-based and the current density-based analyses for systems with multiple (local and global) aromaticity (i.e., aromatic polycyclic hydrocarbons) [60,61]. These differences are because the NICS is affected by coupling contributions from local and global aromatic circuits, making it difficult to assign local, semilocal, and global ring current contributions.

Previously, some of the authors of this work designed a series of ptC global minima composed of carbon and heavier atoms of group 14 of the periodic table [62–64]. The design strategy consisted of replacing three consecutive protons from an aromatic hydrocarbon by one E_2^{4+} fragment ($E = Si-Pb$), favoring the preservation of the π -aromatic circuits of the parent aromatic hydrocarbons (see Scheme 1) [62]. Interestingly, the systems Si_3C_5 , Ge_3C_5 , Si_4C_8 , and Ge_4C_8 ($C_5H_5^-$ and $C_8H_6^{2-}$ derivatives) contain one or two ptCs in their lowest energy structures. The chemical bonding analysis—employing the adaptive natural density partitioning analysis (AdNDP)—suggests that these systems are globally π -aromatic and locally σ -aromatic. This aromatic character was supported by the analysis of the nucleus-independent chemical shift (NICS) [62].

Given the NICS problems mentioned above, in this work we analyze the local and global ring currents in the Si_3C_5 and Si_4C_8 systems. In addition, we analyzed the chemical bonding with the ELF-LOC method, an orbital localization scheme in the domains of the electronic localization function (ELF). The ELF-LOC, like AdNDP, provides information related to electronic delocalization, given its flexibility to identify orbitals distributed in more than two atomic centers. Our results confirm the presence of two delocalization

circuits, one global (π) and one local (σ). More importantly, the global and local ring currents are diatropic and significant (according to the ring current strength, RCS, calculations). These results strongly support these systems' double aromatic character (local and global) and their role in their stability.



Scheme 1. Design strategy of aromatic ptC systems employed in reference [62].

2. Computational Methods

Geometry optimizations were performed at B3LYP [65]/6-311+G* [66,67] level. Vibrational frequencies were evaluated at the same level to confirm the optimized structures as true minima on their potential energy surface using the Gaussian16 program [68]. Cartesian coordinates of the optimized structures are shown in Table S1.

A detailed description of the ELF-LOC algorithm can be found elsewhere [69–72]. In this work, all numerical determinations were performed at the B3LYP level within density functional theory (DFT), using the atomic STO-3G basis sets. The overlap integrals over the ELF regions, required to calculate the localized natural orbitals, were obtained from the GAMESS computational package [73] and a modified version of the ToPMoD program [74]. The orbital localization was performed using our codes [69,70].

Current densities were computed with the GIMIC program [75,76] using the gauge-including atomic orbital (GIAO) [77] method. In the calculations, the magnetic field is directed along the z-axis, i.e., perpendicular to the molecular plane. The unit for current susceptibility is $nA T^{-1}$ and the results are, therefore, independent of the magnitude of the magnetic field. For a qualitative analysis, vector plots of the current density in a plane placed 0.0 and 0.5 Å above the molecular plane were generated. Diatropic (aromatic) and paratropic (antiaromatic) currents are assumed to circle clockwise and counterclockwise, respectively. Current pathways are visualized using Paraview [78,79]. The ring current strengths (RCS), a measure of the net current intensity around the molecular ring, were obtained after considering different integration planes (see Figures S1–S3). The integration planes correspond to cut-off planes perpendicular to the chosen bonds of the molecule and extend horizontally along the ring's plane in 3.6 Å, with 2.6 Å above and below the ring. The two-dimensional Gauss-Lobatto algorithm [76,80] was used to integrate the current passing through an integration plane.

Vector plot visualization of the current density in the plane of the molecule and 0.5 Å above are reported in Figures S1–S5. It is essential to mention that the negative (diatropic) and the positive (paratropic) NICS at the center of the molecules are associated with aromaticity and anti-aromaticity. In contrast, for the RCS, a positive (diatropic) and negative (paratropic) sign correspond to aromatic and anti-aromatic molecules, respectively. For both the NICS and the RCS, values close to zero suggest non-aromatic behavior [81]. Both the NICS and the current density analysis were performed at B3LYP/6-311+G* level.

The NICS were computed using the gauge-including atomic orbital (GIAO) [77] method and dissected into their core, σ , and π contributions, using the natural chemical shielding (NCS) [82] analysis as implemented in the NBO 6.0 program [83]. To evaluate the NICS, we used NICSall, a simple program developed in our group, which is interfaced with the Gaussian program. NICSall helps to prepare the inputs and submits the calculations to generate the data according to the user's requirements. In this work, we computed the NICS in 2D. To do this, we first estimated the box size, which in this case was defined by the sides equal to 1.5 times the length and width of the molecule (centered and placed in the XY plane) by the height (z-axis), taking their lowest value. NICSall prepares the inputs to fill the grid with a step size of 0.2 Å (this is a default value; it could be modified by the user). Finally, NICSall delivers the outputs: text files with the properties (scans, FiPC-NICS) or cube files to plot maps and isosurfaces. The NICS plots were performed with the VisIt 3.0.2 program [84].

It is essential to mention that both the ring currents analysis [76] and the ELF analysis [85,86] are not very dependent on the method or the basis set used in their calculation.

3. Results

For the sake of clarity, our analysis will be divided into two parts: the chemical bonding analysis according to the ELF-LOC method and the global and local aromaticity analysis according to magnetic criteria.

3.1. Chemical Bonding Analysis According to the ELF-LOC Method

The orbital localization provided by the ELF-LOC method reveals a chemical bonding pattern similar to that described by AdNDP, as shown in Figures 1 and 2. In Si_3C_5 and Si_4C_8 , the C_5 and C_8 rings are connected by 2-center 2-electron C-C σ -bonds (2c-2e). For Si_4C_8 , one C-C σ -bond (2c-2e) that splits the C_8 ring into two pentagons is also detected. Additionally, delocalized bonds are detected, three π -bonds in the case of Si_3C_5 and five in Si_4C_8 . Note that in this set, the π -orbitals are distributed over the entire molecular structure. Moreover, delocalized σ -bonds (3c-2e) are also detected in each Si-ptC-Si triangular fragment. These results support global π - and local σ -delocalization, suggesting possible global and local aromaticity according to Hückel's $4n + 2$ rule [87–89].

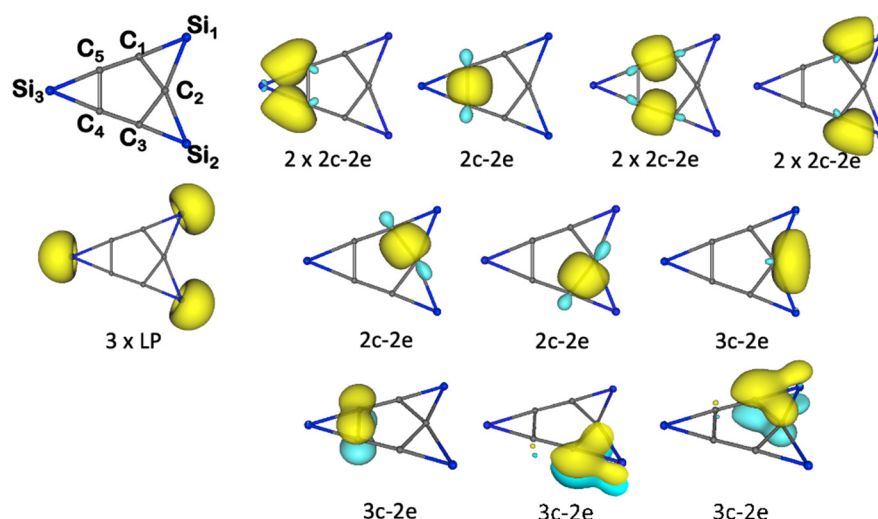


Figure 1. Results of ELF-LOC for Si_3C_5 cluster.

3.2. Current Density Analysis

According to the magnetic criteria, in the presence of an external magnetic field, aromatic (antiaromatic) molecules sustain diatropic (paratropic) currents. In contrast, in nonaromatic molecules, the currents in one direction or the other cancel out, giving a

resultant current strength close to zero [53–55,76,81,90,91]. In this work, we define “local ring current” as the current circuits distributed in a local molecular ring. In contrast, we describe the “global ring current” circuit as distributed around the whole molecule. This assignment was introduced by Sundholm et al. [61] and recently used by our group to highlight the shortcomings of the NICS in assessing the aromaticity of polycyclic systems [92]. Note that Aihara introduced a similar concept to distinguish between different current density pathways [93].

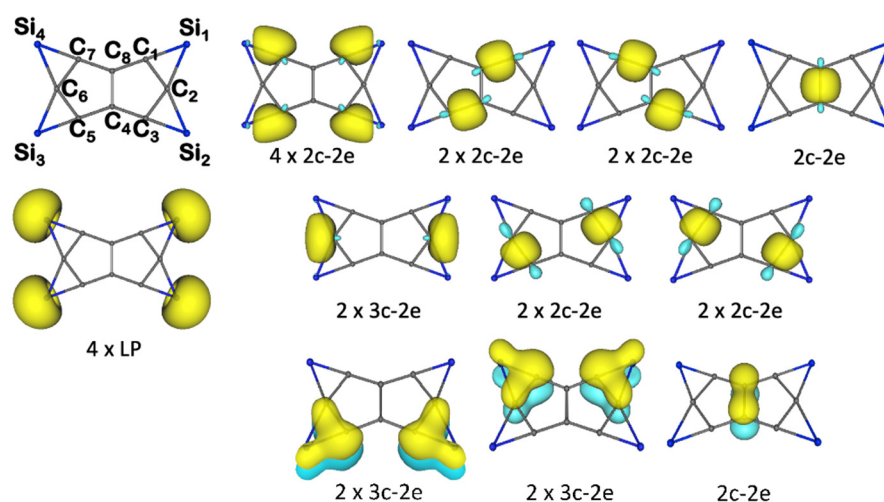


Figure 2. Results of ELF-LOC for Si_4C_8 cluster.

We can glimpse the patterns of current flows by inspecting current density plots. Hence, the magnetically induced current density of Si_3C_5 and Si_4C_8 systems, calculated in a plane located 0.5 \AA above the molecular plane, are shown in Figures 3 and 4 (part a). These plots guide our selection of the integration planes. The different contributions (bond, atomic and ring currents) are defined and quantified by analyzing the integration profiles along the integration planes, see Figures S1 and S2. In this way, it is possible to computationally determine the local and global character of the induced currents. The strength of the local currents (diatropic) is computed and then subtracted from the strength of the diatropic current connecting the local rings to determine the global RCS [61,92]. Accordingly, it has been possible to identify the different delocalization circuits in the studied systems (part b of Figures 3 and 4). In addition, the intensity of each current is also shown in these figures. For the Si_3C_5 system, an intense and paratropic current is detected inside the C_5 ($\text{RCS} = -8.06 \text{ nA/T}$). This ring current is more paratropic than that exhibited by the cyclopentadienyl anion (-3.5 nA T^{-1}), the results of which are shown in Figure S3. A global diatropic ring current with a strength of 12.2 nA T^{-1} is also detected. The latter result is from the delocalization of the six π -electrons and is weaker than that of the cyclopentadienyl anion (14.5 nA T^{-1}). The differences may be due to the effect of the polarization of the π -electron cloud toward the silicon atoms. This hypothesis is supported by analyzing the $\text{Si}_2\text{C}_5\text{H}_2$ system, with one less bridged silicon atom exhibiting a paratropic ($\text{RCS} = -3.6 \text{ nA T}^{-1}$) and diatropic ($\text{RCS} = 13.4 \text{ nA T}^{-1}$) current intensity closer to those of the cyclopentadienyl anion (see Figures S3 and S5). Interestingly, a local diatropic ring current involving the Si-ptC-Si fragment is also detected, in complete agreement with that predicted by AdNDP and the ELF-LOC, which indicated the presence of a σ -delocalized 3c-2e bond. Moreover, the RCS value (5.2 nA/T) suggests that this species has a moderate local σ -aromatic character.

For the case of the Si_4C_8 system (Figure 4), the current density analysis detects two paratropic and local ring currents (within each C_5 ring). Similar to Si_3C_5 , these currents are more paratropic ($\text{RCS} = -4.7 \text{ nA T}^{-1}$) than those of the pentalene dianion ($\text{RCS} = -4.4 \text{ nA T}^{-1}$), whose current density analysis is shown in Figure S4. We also detect

a weak global paratropic ring current ($RCS = -1.6 \text{ nA T}^{-1}$) distributed around the C_8 fragment in addition to an intense global diatropic current ($RCS = 10.4 \text{ A T}^{-1}$). The global diatropic current is less intense than those of the pentalene dianion ($RCS = 10.4 \text{ A T}^{-1}$), presumably because of the polarization of the π -electron cloud toward the silicon. Finally, two local sigma currents are detected, involving the Si-ptC-Si circuits, similar to that exhibited by Si_3C_5 system. Moreover, these currents are of moderate intensity ($RCS = 5.8 \text{ nA T}^{-1}$), leaving in evidence the local sigma aromatic character of these species.

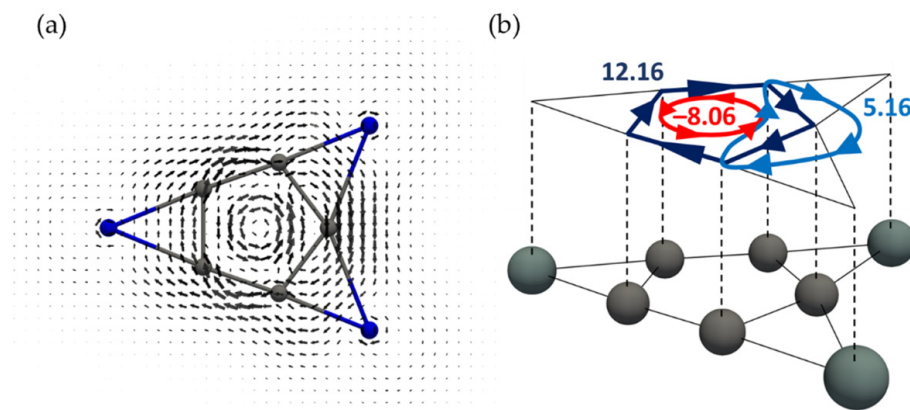


Figure 3. (a) Vector plot visualization of the current density of Si_3C_5 in a plane placed 0.5 \AA above the molecular plane; (b) schematic representation of local and global currents.

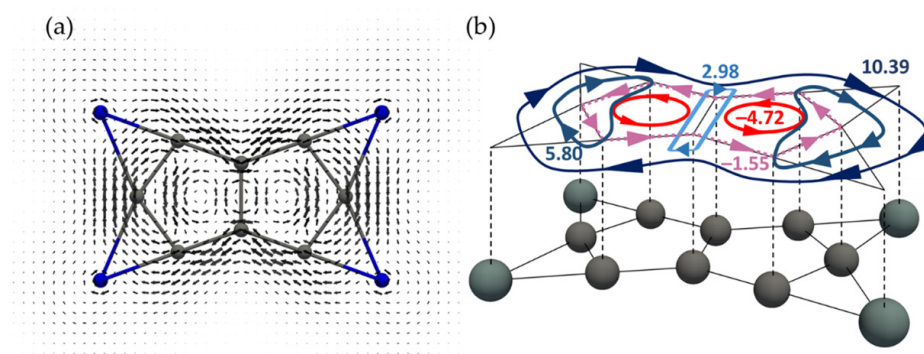


Figure 4. (a) Vector plot visualization of the current density of Si_4C_8 in a plane placed 0.5 \AA above the molecular plane; (b) schematic representation of local and global currents.

3.3. NICS Analysis

Figure 5 shows the σ - and π -components of the $NICS_{zz}$ computed in both the molecular plane and a plane perpendicular to the molecular plane for the Si_3C_5 and Si_4C_8 systems. These plots are in complete agreement with the ring current analysis. The σ -component clearly depicts paratropic regions at the center of the C_5 rings in both Si_3C_5 and Si_4C_8 , in accord with the presence of paratropic ring currents inside these rings. In addition, an intense diatropic region (long-range) centered on the local Si-ptC-Si ring is observed supporting the presence of a local diatropic current in this region. The π -component exhibits a strong diatropic region around the whole Si_3C_5 and Si_4C_8 ring (long-range), in agreement with the presence of a global diatropic ring current. As indicated previously [61,92], the NICS analysis does not allow the identification of all the ring current circuits. However, it is a suitable complement to understand the magnetic behavior of these species and the interpretation of their aromaticity under the magnetic criterion. Figure 6 shows a classical $NICS_{zz}$ analysis, i.e., discrete measurements at the center of the ring and 1.0 \AA above. The values measured in the molecular plane are pretty large (presumably because of the coupling of bond contributions). In contrast, the values above the plane agree with the current strength values measured in the induced current density analysis. In addition,

Figures S6–S8 show an identical NICS_{zz} analysis for Si₂C₅H₂, the cyclopentadienyl anion (C₅H₅[−]), and the pentalene dianion (C₈H₆^{2−}). As seen with the current density analysis, diatropicity due to π -delocalization decreases for species with ptCs, presumably by the electron cloud polarization towards silicon atoms.

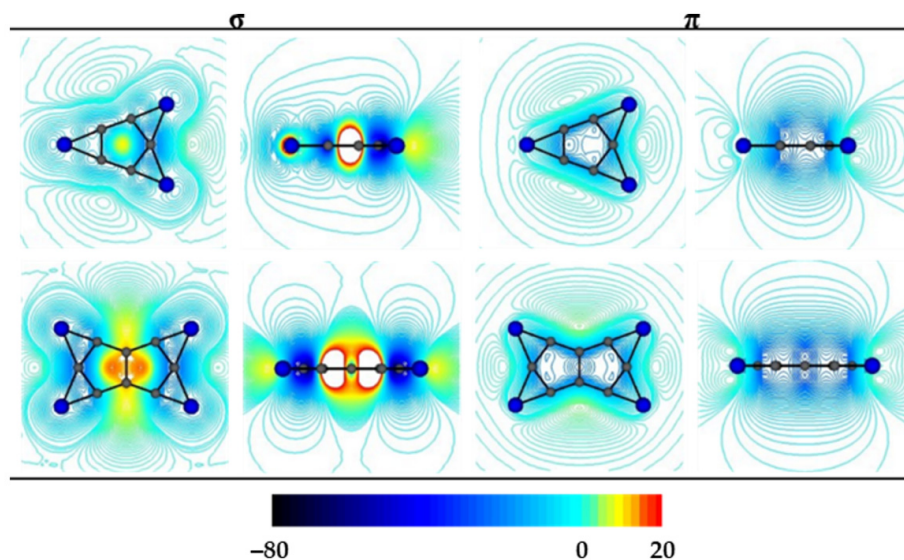


Figure 5. Isolines of the σ - and π -components of NICS_{zz} for the studied molecules (at the GIAO-B3LYP/6-311+G*//B3LYP/6-311+G* level). The isolines are plotted in both the molecular plane (**left**) and a plane perpendicular to the molecular plane (**right**). The color scale at the bottom is in ppm.

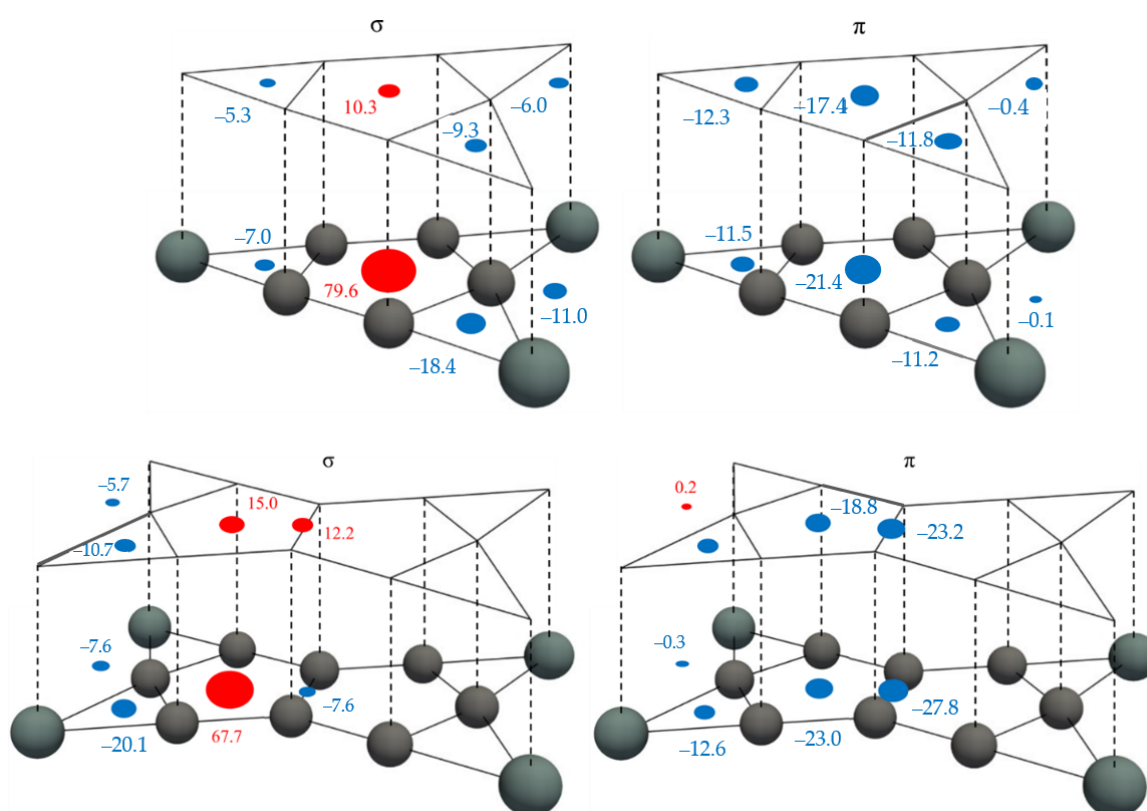


Figure 6. Computed values (in ppm) of σ - and π -components (**left** and **right** sides) of NICS_{zz} at and above the ring centers (local and global) of studied molecules (at the GIAO-B3LYP/6-311+G*//B3LYP/6-311+G* level). The blue/red dots denote diatropic/paratropic character, and the dot size is in line with the NICS_{zz} magnitude.

4. Conclusions

The global (π) and local (σ) aromaticity of Si_3C_5 and Si_4C_8 clusters have been reviewed, employing an orbital localization method (ELF-LOC) and magnetically induced current density analysis.

The ELF-LOC investigation leads to bond descriptions like those reported previously, based on the adaptive natural partitioning analysis (AdNDP) method. These systems show σ - and π -delocalization in agreement with Hückel's rule of $4n + 2$ electrons.

The induced current density analysis identifies global and local aromatic current circuits. In the case of Si_3C_5 , a local paratropic current (of moderate-intensity, $\text{RCS} = -8.1 \text{ nA T}^{-1}$) is detected inside the C_5 ring. However, a diatropic current of higher intensity ($\text{RCS} = 12.16 \text{ nA T}^{-1}$) is also present, which provides a global aromatic character to this species. A local σ -diatropic current involving the Si-ptC-Si fragment is also identified, with moderate intensity ($\text{RCS} = 5.2 \text{ nA T}^{-1}$). These results highlight the double aromatic character of this species. In the case of Si_4C_8 , a weak global paratropic current ($\text{RCS} = -1.5 \text{ nA T}^{-1}$) and an intense global diatropic current ($\text{RCS} = 10.4 \text{ nA T}^{-1}$) are identified. In addition, two local diatropic currents around the Si-ptC-Si rings ($\text{RCS} = 5.8 \text{ nA T}^{-1}$) are also identified. This study highlights the double aromatic character of these clusters and the importance of this delocalization pattern in the stabilization of these species.

The ptC structures of the Si_3C_5 and Si_4C_8 clusters correspond to the global minima and, together with their double aromatic character, suggest that gas-phase experiments could detect these species.

Supplementary Materials: The following are available online at <https://www.mdpi.com/article/10.3390/chemistry3040080/s1>, Table S1: Cartesian coordinates of the studied systems, Figure S1: (a) Vector plot visualization of the current density of Si_3C_5 in a plane placed 0.5 \AA above the molecular plane and top view of integration planes. (b) Integration profiles along the integration planes of Si_3C_5 , Figure S2: (a) Vector plot visualization of the current density of Si_4C_8 in a plane placed 0.5 \AA above the molecular plane and top view of integration planes. (b) Integration profiles along the integration planes of Si_4C_8 , Figure S3: (a) Vector plot visualization of the current density of C_5H_5^- in a plane placed 0.5 \AA above the molecular plane and top view of integration planes (RCS are also reported in nA T^{-1}). (c) Integration profiles along the integration planes of C_5H_5^- , Figure S4: (a) Schematic representation of local and global currents. (b) Vector plot visualization of the current density of $\text{C}_8\text{H}_6^{2-}$ in a plane placed 0.5 \AA above the molecular plane and top view of integration planes. (c) Integration profiles along the integration planes of $\text{C}_8\text{H}_6^{2-}$, Figure S5: (a) Schematic representation of local and global currents. (b) Vector plot visualization of the current density of $\text{Si}_2\text{C}_5\text{H}_2$ in a plane placed 0.5 \AA above the molecular plane and top view of integration planes. (c) Integration profiles along the integration planes of $\text{Si}_2\text{C}_5\text{H}_2$, Figure S6: (a) Computed values (in ppm) of σ - and π -components (left and right sides) of NICS_{zz} at and above the ring centers (local and global) of $\text{Si}_2\text{C}_5\text{H}_2$ (at the GIAO-B3LYP/6-311+G**/B3LYP/6-311+G* level). The blue/red dots denote diatropic/paratropic character, and the dot size is in line with the NICS_{zz} magnitude. (b) Isolines of the σ - and π -components of NICS_{zz} for $\text{Si}_2\text{C}_5\text{H}_2$ (at the GIAO-B3LYP/6-311+G**/B3LYP/6-311+G* level). The isolines are plotted in both the molecular plane (left) and a plane perpendicular to the molecular plane (right). The color scale at the bottom is in ppm, Figure S7: Isolines of the σ - and π -components of NICS_{zz} for both the cyclopentadienyl anion (C_5H_5^-) and the pentalene dianion ($\text{C}_8\text{H}_6^{2-}$) (at the GIAO-B3LYP/6-311+G**/B3LYP/6-311+G* level). The isolines are plotted in both the molecular plane (left) and a plane perpendicular to the molecular plane (right). The color scale at the bottom is in ppm, Figure S8: Computed values (in ppm) of σ - and π -components (left and right sides) of NICS_{zz} at and above the ring centers (local and global) of both the cyclopentadienyl anion (C_5H_5^-) and the pentalene dianion ($\text{C}_8\text{H}_6^{2-}$) (at the GIAO-B3LYP/6-311+G**/B3LYP/6-311+G* level). The blue/red dots denote diatropic/paratropic character, and the dot size is in line with the NICS_{zz} magnitude.

Author Contributions: Conceptualization, J.J.T.-V., V.G. and W.T.; methodology, J.J.T.-V., V.G., D.R.A., O.B.O. and R.B.-G.; computations, J.J.T.-V., V.G., A.V.-E., D.R.A., O.B.O. and R.B.-G.; validation, D.R.A., O.B.O., L.L. and A.T.; formal analysis, W.T., D.R.A., L.L. and A.T.; investigation, J.J.T.-V., V.G., D.R.A. and W.T.; resources, D.R.A., L.L. and W.T.; writing—original draft preparation, J.J.T.-V., W.T. and D.R.A.; writing—review and editing, O.B.O., V.G. and L.L.; supervision, D.R.A. and W.T.; project administration, V.G. and W.T.; funding acquisition, D.R.A., O.B.O. and W.T. All authors have read and agreed to the published version of the manuscript.

Funding: This research was funded by FONDECYT, grant number 1211128, the Universidad de Buenos Aires (Argentina), grant number 20020150100157BA, the Consejo Nacional de Investigaciones Científicas y Técnicas (Argentina), grant numbers PIP 11220130100377CO and PIP 11220130100311CO, and the Agencia Nacional de Promoción Científica y Tecnológica (Argentina), grant number PICT201-0381.

Institutional Review Board Statement: Not applicable.

Informed Consent Statement: Not applicable.

Data Availability Statement: Not applicable.

Acknowledgments: We thank the financial support of the National Agency for Research and Development (ANID) through FONDECYT project 1211128 (W.T.) R.B.-G. acknowledge the financial support of FONDECYT Postdoctorado 3210037. Powered@NLHPC: This research was partially supported by the supercomputing infrastructure of the NLHPC (ECM-02). D.R.A. acknowledges the financial support from the Universidad de Buenos Aires (Grant No. 20020150100157BA). D.R.A. and O.B.O. acknowledge the financial support from the Consejo Nacional de Investigaciones Científicas y Técnicas (Grant Nos. PIP 11220130100377CO and PIP 11220130100311CO), and the Agencia Nacional de Promoción Científica y Tecnológica (Grant No. PICT201-0381), Argentina.

Conflicts of Interest: The authors declare no conflict of interest.

References

1. von Schleyer, P.R.; Jiao, H. What is aromaticity? *Pure Appl. Chem.* **1996**, *68*, 209–218. [[CrossRef](#)]
2. Minkin, V.I.; Glukhovtsev, M.N.; Simkin, B.Y. *Aromaticity and Antiaromaticity*; John Wiley & Sons, Incorporated: Hoboken, NJ, USA, 1994; ISSN 0471593826.
3. Krygowski, T.M.; Cyranski, M.K. Structural Aspects of Aromaticity. *Chem. Rev.* **2001**, *101*, 1385–1420. [[CrossRef](#)]
4. Schleyer, P.V.R. Introduction: Aromaticity. *Chem. Rev.* **2001**, *101*, 1115–1118. [[CrossRef](#)]
5. Boldyrev, A.I.; Wang, L.-S. All-Metal Aromaticity and Antiaromaticity. *Chem. Rev.* **2005**, *105*, 3716–3757. [[CrossRef](#)]
6. Liu, C.; Popov, I.A.; Chen, Z.; Boldyrev, A.I.; Sun, Z. Aromaticity and antiaromaticity in Zintl clusters. *Chem. Eur. J.* **2018**, *24*, 14583–14597. [[CrossRef](#)]
7. Boldyrev, A.I.; Wang, L.-S.S. Beyond organic chemistry: Aromaticity in atomic clusters. *Phys. Chem. Chem. Phys.* **2016**, *18*, 11589–11605. [[CrossRef](#)] [[PubMed](#)]
8. Alexandrova, A.N.; Boldyrev, A.I.; Zhai, H.-J.J.; Wang, L.-S.S. All-boron aromatic clusters as potential new inorganic ligands and building blocks in chemistry. *Coord. Chem. Rev.* **2006**, *250*, 2811–2866. [[CrossRef](#)]
9. Sergeeva, A.P.; Popov, I.A.; Piazza, Z.A.; Li, W.-L.; Romanescu, C.; Wang, L.-S.; Boldyrev, A.I. Understanding boron through size-selected clusters: Structure, chemical bonding, and fluxionality. *Acc. Chem. Res.* **2014**, *47*, 1349–1358. [[CrossRef](#)] [[PubMed](#)]
10. Mercero, J.M.; Boldyrev, A.I.; Merino, G.; Ugalde, J.M. Recent developments and future prospects of all-metal aromatic compounds. *Chem. Soc. Rev.* **2015**, *44*, 6519–6534. [[CrossRef](#)]
11. Huang, X.; Zhai, H.; Kiran, B.; Wang, L. Observation of d-orbital aromaticity. *Angew. Chemie* **2005**, *117*, 7417–7420. [[CrossRef](#)]
12. Tsipis, C.A. DFT study of “all-metal” aromatic compounds. *Coord. Chem. Rev.* **2005**, *249*, 2740–2762. [[CrossRef](#)]
13. Rabanal-León, W.; Vásquez-Espinal, A.; Yañez, O.; Pino-Rios, R.; Arratia-Pérez, R.; Alvarez-Thon, L.; Torres-Vega, J.; Tiznado, W. Aromaticity of $[M_3(\mu-X)_3X_6]^{0/2-}$ (M= Re and Tc, X= Cl, Br, I) Clusters Confirmed by Ring Current Analysis and Induced Magnetic Field. *Eur. J. Inorg. Chem.* **2018**, *2018*, 3312–3319. [[CrossRef](#)]
14. Vásquez-Espinal, A.; Pino-Rios, R.; Alvarez-Thon, L.; Rabanal-León, W.A.; Torres-Vega, J.J.; Arratia-Pérez, R.; Tiznado, W. New Insights into $Re_3(\mu-Cl)_3Cl_6$ Aromaticity. Evidence of σ - and π -Diatropicity. *J. Phys. Chem. Lett.* **2015**, *6*, 4326–4330. [[CrossRef](#)]
15. Bleeke, J.R.; Behm, R.; Xie, Y.-F.; Chiang, M.Y.; Robinson, K.D.; Beatty, A.M. Synthesis, Structure, Spectroscopy, and Reactivity of a Metallabenzene¹. *Organometallics* **1997**, *16*, 606–623. [[CrossRef](#)]
16. Bleeke, J.R.; Xie, Y.F.; Peng, W.J.; Chiang, M. Metallabenzene: Synthesis, structure, and spectroscopy of a 1-irida-3, 5-dimethylbenzene complex. *J. Am. Chem. Soc.* **1989**, *111*, 4118–4120. [[CrossRef](#)]
17. Bleeke, J.R. Metallabenzenes. *Chem. Rev.* **2001**, *101*, 1205–1228. [[CrossRef](#)] [[PubMed](#)]
18. Fernández, I.; Frenking, G.; Merino, G. Aromaticity of metallabenzene and related compounds. *Chem. Soc. Rev.* **2015**, *44*, 6452–6463. [[CrossRef](#)] [[PubMed](#)]

19. Vásquez-Espinal, A.; Poater, J.; Solà, M.; Tiznado, W.; Islas, R. Testing the effectiveness of the isoelectronic substitution principle through the transformation of aromatic osmathiophene derivatives into their inorganic analogues. *New J. Chem.* **2017**, *41*, 1168–1178. [[CrossRef](#)]
20. Popov, I.A.; Bozhenko, K.V.; Boldyrev, A.I. Is graphene aromatic? *Nano Res.* **2012**, *5*, 117–123. [[CrossRef](#)]
21. Zubarev, D.Y.; Boldyrev, A.I. Revealing intuitively assessable chemical bonding patterns in organic aromatic molecules via adaptive natural density partitioning. *J. Org. Chem.* **2008**, *73*, 9251–9258. [[CrossRef](#)]
22. Tkachenko, N.V.; Boldyrev, A.I. Multiple local σ -aromaticity of nonagermanide clusters. *Chem. Sci.* **2019**, *10*, 5761–5765. [[CrossRef](#)]
23. Hoffmann, R.; Alder, R.W.; Wilcox, C.F. Planar tetracoordinate carbon. *J. Am. Chem. Soc.* **1970**, *92*, 4992–4993. [[CrossRef](#)]
24. Erker, G. Planar-Tetracoordinate Carbon: Making Stable Anti-van't Hoff/LeBel Compounds. *Comments Inorg. Chem.* **1992**, *13*, 111–131. [[CrossRef](#)]
25. Röttger, D.; Erker, G. Compounds Containing Planar-Tetracoordinate Carbon. *Angew. Chemie Int. Ed. English* **1997**, *36*, 812–827. [[CrossRef](#)]
26. Siebert, W.; Gunale, A. Compounds containing a planar-tetracoordinate carbon atom as analogues of planar methane. *Chem. Soc. Rev.* **1999**, *28*, 367–371. [[CrossRef](#)]
27. Keese, R. Carbon flatland: Planar tetracoordinate carbon and fenestranes. *Chem. Rev.* **2006**, *106*, 4787–4808. [[CrossRef](#)] [[PubMed](#)]
28. Merino, G.; Méndez-Rojas, M.A.; Vela, A.; Heine, T. Recent advances in planar tetracoordinate carbon chemistry. *J. Comput. Chem.* **2007**, *28*, 362–372. [[CrossRef](#)] [[PubMed](#)]
29. Zhang, X.; Ding, Y. Computational prediction of a global planar penta-coordinate carbon structure CA_4Ga^+ . *Comput. Theor. Chem.* **2014**, *1048*, 18–24. [[CrossRef](#)]
30. Li, X.; Zhang, H.; Wang, L.; Geske, G.D.; Boldyrev, A.I. Pentaatomic tetracoordinate planar carbon, $[CA_4]^{2-}$: A new structural unit and its salt complexes. *Angew. Chemie Int. Ed.* **2000**, *39*, 3630–3632. [[CrossRef](#)]
31. Wang, Z.-X.; von Ragué Schleyer, P. Construction principles of “hyparenes”: Families of molecules with planar pentacoordinate carbons. *Science* **2001**, *292*, 2465–2469. [[CrossRef](#)]
32. Wang, Y.; Li, F.; Li, Y.; Chen, Z. Semi-metallic Be_5C_2 monolayer global minimum with quasi-planar pentacoordinate carbons and negative Poisson's ratio. *Nat. Commun.* **2016**, *7*, 11488. [[CrossRef](#)]
33. Pan, S.; Cabellos, J.L.; Orozco-Ic, M.; Chattaraj, P.K.; Zhao, L.; Merino, G. Planar pentacoordinate carbon in CGa_5^+ derivatives. *Phys. Chem. Chem. Phys.* **2018**, *20*, 12350–12355. [[CrossRef](#)] [[PubMed](#)]
34. Pei, Y.; An, W.; Ito, K.; Schleyer, P.V.R.; Zeng, X.C. Planar pentacoordinate carbon in CA_5^+ : A global minimum. *J. Am. Chem. Soc.* **2008**, *130*, 10394–10400. [[CrossRef](#)] [[PubMed](#)]
35. Vassilev-Galindo, V.; Pan, S.; Donald, K.J.; Merino, G. Planar pentacoordinate carbons. *Nat. Rev. Chem.* **2018**, *2*, 114. [[CrossRef](#)]
36. Grande-Aztatzi, R.; Cabellos, J.L.; Islas, R.; Infante, I.; Mercero, J.M.; Restrepo, A.; Merino, G. Planar pentacoordinate carbons in CBe_5^{4-} derivatives. *Phys. Chem. Chem. Phys.* **2015**, *17*, 4620–4624. [[CrossRef](#)]
37. Zhao, X.-F.; Bian, J.-H.; Huang, F.; Yuan, C.; Wang, Q.; Liu, P.; Li, D.; Wang, X.; Wu, Y.-B. Stabilization of beryllium-containing planar pentacoordinate carbon species through attaching hydrogen atoms. *RSC Adv.* **2018**, *8*, 36521–36526. [[CrossRef](#)]
38. Cui, Z.; Vassilev-Galindo, V.; Cabellos, J.L.; Osorio, E.; Orozco, M.; Pan, S.; Ding, Y.; Merino, G. Planar pentacoordinate carbon atoms embedded in a metallocene framework. *Chem. Commun.* **2017**, *53*, 138–141. [[CrossRef](#)]
39. Wu, Y.-B.; Duan, Y.; Lu, G.; Lu, H.-G.; Yang, P.; von Rague Schleyer, P.; Merino, G.; Islas, R.; Wang, Z.-X. D_{3h} $CN_3Be_3^+$ and $CO_3Li_3^+$: Viable planar hexacoordinate carbon prototypes. *Phys. Chem. Chem. Phys.* **2012**, *14*, 14760–14763. [[CrossRef](#)]
40. Exner, K.; von Ragué Schleyer, P. Planar hexacoordinate carbon: A viable possibility. *Science.* **2000**, *290*, 1937–1940. [[CrossRef](#)]
41. Parra, L.L.; Diego, L.; Yañez, O.; Inostroza, D.; Barroso, J.; Espinal, A.V.; Merino, G.; Tiznado, W. Planar Hexacoordinate Carbons: Half Covalent, Half Ionic. *Angew. Chem. Int. Ed. Engl.* **2021**, *60*, 8700–8704. [[CrossRef](#)]
42. Li, Y.; Liao, Y.; Chen, Z. Be_2C monolayer with quasi-planar hexacoordinate carbons: A global minimum structure. *Angew. Chemie* **2014**, *126*, 7376–7380. [[CrossRef](#)]
43. Feixas, F.; Matito, E.; Poater, J.; Sola, M. Quantifying aromaticity with electron delocalisation measures. *Chem. Soc. Rev.* **2015**, *44*, 6434–6451. [[CrossRef](#)] [[PubMed](#)]
44. Gomes, J.; Mallion, R.B. Aromaticity and ring currents. *Chem. Rev.* **2001**, *101*, 1349–1384. [[CrossRef](#)]
45. Mitchell, R.H. Measuring aromaticity by NMR. *Chem. Rev.* **2001**, *101*, 1301–1316. [[CrossRef](#)]
46. Cyranski, M.K.; Krygowski, T.M.; Katritzky, A.R.; Schleyer, P.V.R. To what extent can aromaticity be defined uniquely? *J. Org. Chem.* **2002**, *67*, 1333–1338. [[CrossRef](#)] [[PubMed](#)]
47. Randić, M. Aromaticity of polycyclic conjugated hydrocarbons. *Chem. Rev.* **2003**, *103*, 3449–3606. [[CrossRef](#)]
48. Balaban, A.T.; Oniciu, D.C.; Katritzky, A.R. Aromaticity as a cornerstone of heterocyclic chemistry. *Chem. Rev.* **2004**, *104*, 2777–2812. [[CrossRef](#)]
49. McWeeny, R. Ring currents and proton magnetic resonance in aromatic molecules. *Mol. Phys.* **1958**, *1*, 311–321. [[CrossRef](#)]
50. Pople, J.A. Molecular orbital theory of aromatic ring currents. *Mol. Phys.* **1958**, *1*, 175–180. [[CrossRef](#)]
51. Pauling, L. The diamagnetic anisotropy of aromatic molecules. *J. Chem. Phys.* **1936**, *4*, 673–677. [[CrossRef](#)]
52. Kumar, C.; Fliegl, H.; Sundholm, D. Relation Between Ring Currents and Hydrogenation Enthalpies for Assessing the Degree of Aromaticity. *J. Phys. Chem. A* **2017**, *121*, 7282–7289. [[CrossRef](#)]
53. Ligabue, A.; Pincelli, U.; Lazzeretti, P.; Zanasi, R. Current density maps, magnetizability, and nuclear magnetic shielding tensors for anthracene, phenanthrene, and triphenylene. *J. Am. Chem. Soc.* **1999**, *121*, 5513–5518. [[CrossRef](#)]

54. Monaco, G.; Fowler, P.W.; Lillington, M.; Zanasi, R. Designing paramagnetic circulenes. *Angew. Chemie* **2007**, *119*, 1921–1924. [[CrossRef](#)]
55. Lazzeretti, P. Assessment of aromaticity via molecular response properties. *Phys. Chem. Chem. Phys.* **2004**, *6*, 217–223. [[CrossRef](#)]
56. Schleyer, P.V.R.; Maerker, C.; Dransfeld, A.; Jiao, H.; van Eikema Hommes, N.J.R. Nucleus-independent chemical shifts: A simple and efficient aromaticity probe. *J. Am. Chem. Soc.* **1996**, *118*, 6317–6318. [[CrossRef](#)]
57. Haddon, R.C. The application of the Biot-Savart law to the ring current analysis of proton chemical shifts—II: An approach to aromatic character in the annulenes. *Tetrahedron* **1972**, *28*, 3635–3655. [[CrossRef](#)]
58. Báez-Grez, R.; Rabanal-León, W.A.; Alvarez-Thon, L.; Ruiz, L.; Tiznado, W.; Pino-Rios, R. Aromaticity in heterocyclic analogues of benzene: Dissected NICS and current density analysis. *J. Phys. Org. Chem.* **2019**, *32*, e3823. [[CrossRef](#)]
59. Báez-Grez, R.; Ruiz, L.; Pino-Rios, R.; Tiznado, W. Which NICS method is most consistent with ring current analysis? Assessment in simple monocycles. *RSC Adv.* **2018**, *8*, 13446–13453. [[CrossRef](#)]
60. Poater, J.; Solà, M.; Viglione, R.G.; Zanasi, R. Local aromaticity of the six-membered rings in pyracylene. A difficult case for the NICS indicator of aromaticity. *J. Org. Chem.* **2004**, *69*, 7537–7542. [[CrossRef](#)] [[PubMed](#)]
61. Sundholm, D.; Berger, R.J.F.; Fliegl, H. Analysis of the magnetically induced current density of molecules consisting of annelated aromatic and antiaromatic hydrocarbon rings. *Phys. Chem. Chem. Phys.* **2016**, *18*, 15934–15942. [[CrossRef](#)]
62. Yañez, O.; Vásquez-Espinal, A.; Báez-Grez, R.; Rabanal-León, W.A.; Osorio, E.; Ruiz, L.; Tiznado, W. Carbon rings decorated with group 14 elements: New aromatic clusters containing planar tetracoordinate carbon. *New J. Chem.* **2019**, *43*, 6781–6785. [[CrossRef](#)]
63. Yañez, O.; Báez-Grez, R.; Garza, J.; Pan, S.; Barroso, J.; Vásquez-Espinal, A.; Merino, G.; Tiznado, W. Embedding a Planar Hypercoordinate Carbon Atom into a $[4n+2]$ π -System. *ChemPhysChem* **2020**, *21*, 145–148. [[CrossRef](#)] [[PubMed](#)]
64. Yañez, O.; Vásquez-Espinal, A.; Pino-Rios, R.; Ferraro, F.; Pan, S.; Osorio, E.; Merino, G.; Tiznado, W. Exploiting electronic strategies to stabilize a planar tetracoordinate carbon in cyclic aromatic hydrocarbons. *Chem. Commun.* **2017**, *53*, 12112–12115. [[CrossRef](#)]
65. Becke, A.D. Becke's three parameter hybrid method using the LYP correlation functional. *J. Chem. Phys.* **1993**, *98*, 5648–5652. [[CrossRef](#)]
66. Ditchfield, R.; Hehre, W.J.; Pople, J.A. Self-consistent molecular-orbital methods. IX. An extended Gaussian-type basis for molecular-orbital studies of organic molecules. *J. Chem. Phys.* **1971**, *54*, 724–728. [[CrossRef](#)]
67. Hehre, W.J.; Ditchfield, R.; Pople, J.A. Self-consistent molecular orbital methods. XII. Further extensions of Gaussian-type basis sets for use in molecular orbital studies of organic molecules. *J. Chem. Phys.* **1972**, *56*, 2257–2261. [[CrossRef](#)]
68. Frisch, M.J.; Trucks, G.W.; Schlegel, H.B.; Scuseria, G.E.; Robb, M.A.; Cheeseman, J.R.; Scalmani, G.; Barone, V.; Petersson, G.A.; Nakatsuji, H.; et al. *Gaussian 16, Revis. C.01*; Gaussian, Inc.: Wallingford, CT, USA.
69. Oña, O.B.; Alcoba, D.R.; Tiznado, W.; Torre, A.; Lain, L. An orbital localization criterion based on the topological analysis of the electron localization function. *Int. J. Quantum Chem.* **2013**, *113*, 1401–1408. [[CrossRef](#)]
70. Oña, O.B.; Alcoba, D.R.; Torre, A.; Lain, L.; Torres-Vega, J.J.; Tiznado, W. Orbital Localization Criterion as a Complementary Tool in the Bonding Analysis by Means of Electron Localization Function: Study of the $\text{Si}_n(\text{BH})_{5-n}^{2-}$ ($n = 0-5$) Clusters. *J. Phys. Chem. A* **2013**, *117*, 12953–12958. [[CrossRef](#)]
71. Alcoba, D.R.; Oña, O.B.; Torre, A.; Lain, L.; Tiznado, W. An orbital localization criterion based on the topological analysis of the electron localization function at correlated level. *Int. J. Quantum Chem.* **2018**, *118*, e25588. [[CrossRef](#)]
72. Oña, O.B.; Torres-Vega, J.J.; Torre, A.; Lain, L.; Alcoba, D.R.; Vásquez-Espinal, A.; Tiznado, W. Chemical bonding analysis in boron clusters by means of localized orbitals according to the electron localization function topology. *Theor. Chem. Acc.* **2015**, *134*, 1–9. [[CrossRef](#)]
73. Schmidt, M.W.; Baldridge, K.K.; Boatz, J.A.; Elbert, S.T.; Gordon, M.S.; Jensen, J.H.; Koseki, S.; Matsunaga, N.; Nguyen, K.A.; Su, S. General atomic and molecular electronic structure system. *J. Comput. Chem.* **1993**, *14*, 1347–1363. [[CrossRef](#)]
74. Noury, S.; Krokidis, X.; Fuster, F.; Silvi, B. Computational tools for the electron localization function topological analysis. *Comput. Chem.* **1999**, *23*, 597–604. [[CrossRef](#)]
75. Fliegl, H.; Taubert, S.; Lehtonen, O.; Sundholm, D. The gauge including magnetically induced current method. *Phys. Chem. Chem. Phys.* **2011**, *13*, 20500–20518. [[CrossRef](#)] [[PubMed](#)]
76. Jusélius, J.; Sundholm, D.; Gauss, J. Calculation of current densities using gauge-including atomic orbitals. *J. Chem. Phys.* **2004**, *121*, 3952–3963. [[CrossRef](#)]
77. Wolinski, K.; Hinton, J.F.; Pulay, P. Efficient implementation of the gauge-independent atomic orbital method for NMR chemical shift calculations. *J. Am. Chem. Soc.* **1990**, *112*, 8251–8260. [[CrossRef](#)]
78. Ahrens, J.; Geveci, B.; Law, C. Paraview: An end-user tool for large data visualization. *Vis. Handb.* **2005**, 717. [[CrossRef](#)]
79. Ayachit, U. *The ParaView Guide: A Parallel Visualization Application*; Kitware, Inc.: Saratoga County, NY, USA, 2015; ISBN 1930934300.
80. Abramowitz, M. *Handbook of Mathematical Functions, With Formulas, Graphs, and Mathematical Tables*; Dover Publications, Inc.: New York, NY, USA, 1974; ISBN 0486612724.
81. Sundholm, D.; Fliegl, H.; Berger, R.J.F. Calculations of magnetically induced current densities: Theory and applications. *Wiley Interdiscip. Rev. Comput. Mol. Sci.* **2016**, *6*, 639–678. [[CrossRef](#)]
82. Bohmann, J.A.; Weinhold, F.; Farrar, T.C. Natural chemical shielding analysis of nuclear magnetic resonance shielding tensors from gauge-including atomic orbital calculations. *J. Chem. Phys.* **1997**, *107*, 1173–1184. [[CrossRef](#)]

83. Glendening, E.D.; Badenhoop, J.K.; Reed, A.E.; Carpenter, J.E.; Bohmann, J.A.; Morales, C.M.; Landis, C.R.; Weinhold, F. *Natural Bond Orbital Analysis Program: NBO 6.0*; Theoretical Chemistry Institute and Department of Chemistry, University of Wisconsin: Madison, WI, USA, 2013.
84. Childs, H.; Brugger, E.; Whitlock, B.; Meredith, J.; Ahern, S.; Pugmire, D.; Biagas, K.; Miller, M.; Harrison, C.; Weber, G.H.; et al. VisIt: An End-User Tool For Visualizing and Analyzing Very Large Data. In *High Performance Visualization—Enabling Extreme-Scale Scientific Insight*; CRC Press: Boca Raton, FL, USA, 2012; pp. 357–372.
85. Llusar, R.; Beltrán, A.; Andrés, J.; Noury, S.; Silvi, B. Topological analysis of electron density in depleted homopolar chemical bonds. *J. Comput. Chem.* **1999**, *20*, 1517–1526. [[CrossRef](#)]
86. Silvi, B.; Savin, A. Classification of chemical bonds based on topological analysis of electron localization functions. *Nature* **1994**, *371*, 683–686. [[CrossRef](#)]
87. Hückel, E. Quantentheoretische Beiträge zum Benzolproblem. *Zeitschrift Phys.* **1931**, *70*, 204–286. [[CrossRef](#)]
88. Hückel, E. Quantentheoretische Beiträge zum Benzolproblem. *Zeitschrift Phys.* **1931**, *72*, 310–337. [[CrossRef](#)]
89. Hückel, E. Zur Quantentheorie der Doppelbindung. *Zeitschrift Phys.* **1930**, *60*, 423–456. [[CrossRef](#)]
90. Lazzeretti, P. Ring currents. *Prog. Nucl. Magn. Reson. Spectrosc.* **2000**, *36*, 1–88. [[CrossRef](#)]
91. Juse, J.; Sundholm, D. Ab initio determination of the induced ring current in aromatic molecules. *Phys. Chem. Chem. Phys.* **1999**, *1*, 3429–3435.
92. Inostroza, D.; García, V.; Yañez, O.; Torres-Vega, J.J.; Vásquez-Espinal, A.; Pino-Rios, R.; Báez-Grez, R.; Tiznado, W. On the NICS limitations to predict local and global current pathways in polycyclic systems. *New J. Chem.* **2021**, *45*, 8345–8351. [[CrossRef](#)]
93. Aihara, J. Circuit resonance energy: A key quantity that links energetic and magnetic criteria of aromaticity. *J. Am. Chem. Soc.* **2006**, *128*, 2873–2879. [[CrossRef](#)] [[PubMed](#)]